



A novel low temperature sol–gel synthesis process for thermally stable nano crystalline hydroxyapatite

Feray Bakan^{a,b,*}, Oral Laçın^b, Hanifi Sarac^b

^a Sabancı University, Nanotechnology Research and Application Center, Istanbul, Turkey

^b Atatürk University, Department of Chemical Engineering, Erzurum, Turkey

ARTICLE INFO

Article history:

Received 24 April 2012

Received in revised form 24 August 2012

Accepted 25 August 2012

Available online 31 August 2012

Keywords:

Biomaterials
Sol–gel growth
Hydroxyapatite

ABSTRACT

Hydroxyapatite is a class of calcium phosphate-based bioceramic, frequently used as a bone graft substitute due to its chemical and structural similarity with natural bone mineral. In the present investigation, a novel method is developed to synthesize pure, stable, stoichiometric nano crystalline hydroxyapatite (HA: $\text{Ca}_{10}(\text{PO}_4)_6(\text{OH})_2$) at room temperature via alcohol based sol–gel route using $\text{Ca}(\text{NO}_3)_2 \cdot 4\text{H}_2\text{O}$ and $\text{NH}_4\text{H}_2\text{PO}_4$ as calcium and phosphorous precursors, respectively. We have developed a novel method for the synthesis of nanometer sized HA particles (HAp) without using any catalyst and was synthesized without any grinding process during the gel formation. Polycrystalline HAp synthesized by this new technique is characterized by XRD, FTIR, TGA, SEM and TEM.

© 2012 Elsevier B.V. All rights reserved.

1. Introduction

In past few decades, synthetic hydroxyapatite (HA: $\text{Ca}_{10}(\text{PO}_4)_6(\text{OH})_2$) has been extensively used as a bone substitute material due to its chemical and structural similarity with natural bone mineral [1–3]. The HA which can be derived from natural sources or synthesized by various methods is regarded as a good bioactive substance, since it forms a strong chemical bond with the host bone tissue, and hence it is recognized as a good bone graft material. However, the particle size of the natural apatite in the bone mineral is in the nano scale with a very large surface area. Synthetic HA particles (HAp) on the contrary have low surface area and present strong bonding properties [4]. Many researchers have attempted to engineer its properties such as bioactivity, solubility and sinterability by controlling its composition, morphology and particle size [5–7].

During recent years, a number of different techniques, such as precipitation, sol–gel, hydrothermal, multiple emulsion, biomimetic deposition, electrodeposition [8–10], have been applied for the synthesis of HA. The sol–gel method is preferred due to its low synthesis temperature, high product purity, homogenous molecular mixing and the ability to generate nano sized particles compared to other alternatives [11].

Sol–gel method for the preparation of HAp can usually form fine-grain microstructure containing a mixture of nano-to-submicron particles with crystalline structure. It has been reported that these crystals are very efficient to improve the contact and stability at the

artificial/natural bone interface observed *in vitro* and *in vivo* environments [12].

The synthesis of HAp by sol–gel method requires a correct molar ratio of 1.67:1 between Ca and P in the final product [13]. Moreover there are a lot of different calcium and phosphorus precursors used for HAp synthesis, as reported sol–gel processes in the literature. Besides, bioactivity of Ca–P based materials is dependent on many factors such as the synthesis procedure, precursor reagents, impurity contents, crystal size and morphology, concentration and mixture order of reagents, pH and temperature. Selection of the route of synthesis depends on the application [3,5,11–13].

In this work, a novel, low temperature alcohol based sol–gel method for the synthesis of pure nano-HAp was developed using $\text{Ca}(\text{NO}_3)_2 \cdot 4\text{H}_2\text{O}$ and $\text{NH}_4\text{H}_2\text{PO}_4$ as calcium (Ca) and phosphorus (P) precursors. The advantages of this novel technique over the previous studies [3,14–26] concerning sol–gel synthesis of HAp most importantly include: (a) carrying out the reaction at room temperature, (b) obtaining the gel formation without any dispersant and (c) forming nano sized HAp without using any grinding process.

The structure of nano-HAp synthesized with this novel method was investigated using FTIR, XRD, DTA/TGA, SEM and TEM. We have found that pure HAp phase with hexagonal-crystal structure could be synthesized at room temperature with nanometer size.

2. Materials and methods

2.1. Sol–gel processing

A very simple method was set up to obtain nano-HAp. The flow chart given in Fig. 1 outlines the experimental procedure used to

* Corresponding author at: Sabancı University, Nanotechnology Research and Application Center, Istanbul, Turkey. Tel.: +90 2164839000 2417; fax: +90 2164839885.

E-mail address: feraybakan@sabanciuniv.edu (F. Bakan).

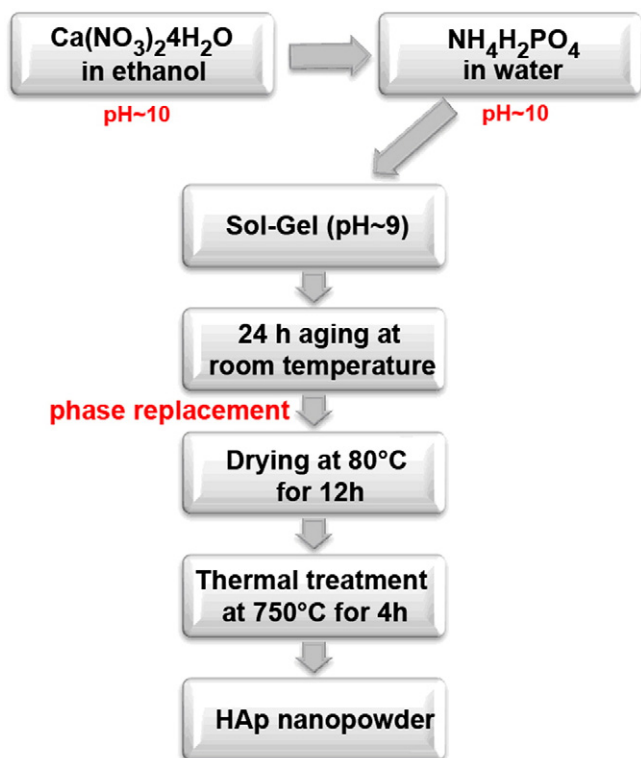
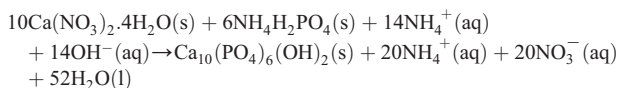


Fig. 1. The flow chart of HAp preparation.

generate the nano-HAp. In the synthesis, $\text{Ca}(\text{NO}_3)_2 \cdot 4\text{H}_2\text{O}$ (Merck) and $\text{NH}_4\text{H}_2\text{PO}_4$ (Sigma Aldrich) were used as starting Ca and P precursors. Ammonia (NH_3 , Merck) was used to adjust the pH of the solution. The following synthesis reaction was carried out:



1.67 M $\text{Ca}(\text{NO}_3)_2 \cdot 4\text{H}_2\text{O}$ solution in ethanol (pH 10) was added at a constant rate of 3 mL min^{-1} using a peristaltic pump into the 1 M $\text{NH}_4\text{H}_2\text{PO}_4$ solution (Ca/P = 1.67) under vigorous stirring at room

temperature. After the white precipitate solution was obtained, this is aged for 12, 24 and 48 h at room temperature.

The gel obtained after aging process was filtered and washed repeatedly using double distilled water to remove $\text{NH}_4^+(\text{aq})$ and $\text{NO}_3^-(\text{aq})$. In addition, the gel was washed repeatedly using pure acetone (Merck) to change the phase while preventing the agglomeration. The filter cake obtained by this process was then dried at 80°C for 12 h in an oven and the dried powder was calcined at 750°C for 4 h, using an electrical furnace, employing a heating rate of $10^\circ\text{C min}^{-1}$ in air.

2.2. Characterization

The dried samples were first characterized by Fourier transform infrared spectroscopy (FTIR, Perkin-Elmer Pyris1) in the range of $400\text{--}4000 \text{ cm}^{-1}$ to determine the stoichiometry deviations, i.e. the presence of anions partially substituting PO_4^{3-} and/or OH^- groups of the nano-HAp. To investigate the phase composition and crystallinity of the sintered nano-HAp, the X-ray diffraction (XRD) analysis was performed at a Rigaku, Dmax 2000 using a $\text{CuK}\alpha$ radiation ($\lambda = 0.1542 \text{ \AA}$), with the step scanning mode, applying a tube voltage of 40 kV and a tube current of 50 mA. The XRD patterns were then recorded in the 2θ range of $20^\circ\text{--}60^\circ$, with a step size of 0.04° and a step duration of 0.5 s. Peak broadening in the XRD data can be informative to estimate the crystallite size in a direction perpendicular to the crystallographic plane, based on the Scherrer's formula as follows [27]:

$$D = 0.89\lambda / \beta \cos\theta \quad (1)$$

where D is the crystallite size (nm), λ is the wavelength of X-ray beam (nm), β is the full width at the half maximum of the HAp (002) line (rad), and θ is the diffraction angle ($^\circ$).

The thermal decomposition of the nano-HAp was studied in nitrogen atmosphere by using thermo gravimetric analysis (TGA) with NETZSCH STA 409 PC Luxx TGA performed between 30°C and 1200°C , heating with a rate of $20^\circ\text{C min}^{-1}$.

The particle size of the as-synthesized pure nano-HAp is also measured using scanning electron microscopy (SEM) with a JEOL JSM-6335F Field Emission SEM. The agglomeration is also observed using the SEM.

Transmission electron microscopy (TEM) investigations were performed with a JEOL JEM 2100 HRTEM operating at 200 kV (LaB₆ filament). TEM images were recorded by using a Gatan Model 694 Slow Scan CCD camera, where the morphology and the particle size

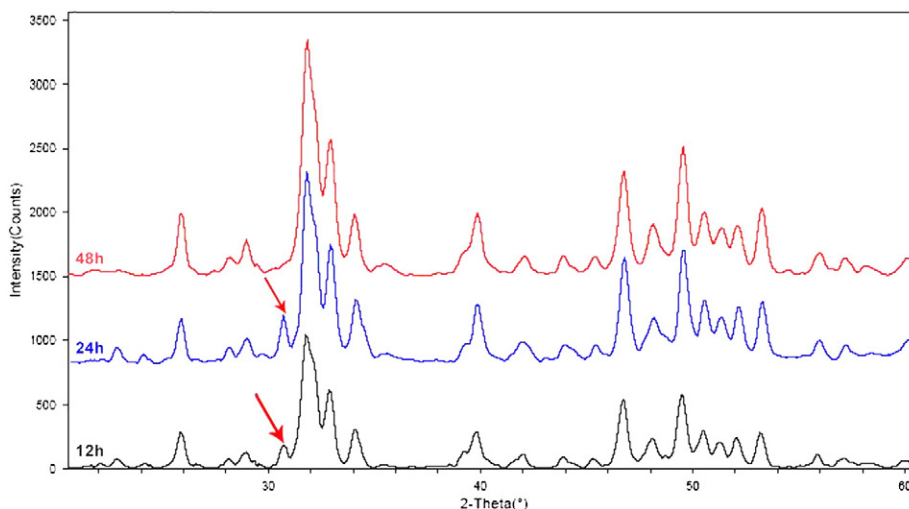


Fig. 2. The effect of aging time on the crystal structure of HAp sintered at 750°C in air, measured by XRD.

Table 1

The effect of aging time on the lattice parameters, unit cell volume and the crystallite size of the synthesized HAp sample.

Sample	Lattice parameter (Å)		Unit cell volume (Å) ³	Crystallite size (nm) ^b
	a ₀	c ₀		
Reference HAp ^a	9.418	6.888	528.80	
HAp, 12 h aging	9.383	6.875	524.16	26.77
HAp, 24 h aging	9.405	6.882	527.13	26.46
HAp, 48 h aging	9.418	6.871	527.75	33.47

^a International Centre for Diffraction Data (ICDD)-(JCSd 09-432).

^b Calculated from Scherrer equation (Eq. (1)).

of the dried and sintered nano-HAp samples were observed and analyzed.

3. Results and discussions

3.1. XRD patterns

The XRD patterns of the nano-HAp crystals sintered at 750 °C are shown in Fig. 2 for different aging periods. Phase analysis was performed using PDF card no. 009-0432 for HA and 29-0359 for Ca₃PO₄ (β-TCP), providing information in the 2θ range of 20°–60°. Phase analysis revealed that all major peaks of HAp were present in the synthesized powder. The peak which was observed at 31.71° in the XRD patterns of the samples that were synthesized using 12 h and 24 h aging times corresponds to (034) Miller plane, corresponds to the β-TCP phase with JCPDS number 29-0359. This could suggest that a small amount of β-TCP might be formed as an impurity phase together with HAp. After 48 h aging time, β-TCP phase gradually disappeared and the apatite phase was found to be predominant. These observations finally suggest that the critical aging time is essentially required for the sol to obtain phase-pure apatite samples. As seen in the XRD patterns, the broad peaks highlighted the smaller size of the crystallite/particle in the powder. As the diffraction peak at 25.9° corresponding to (002) Miller plane is an isolated sharp one, it was selected for the calculation of the crystalline size. This corresponds to the crystal growth following the c-axis of the hexagonal HAp structure, as reported in the literature [28]. The lattice parameters, unit cell volumes and the calculated mean particle sizes of the samples are given in Table 1. The list of the major peaks observed in the X-ray powder diffraction pattern of HAp synthesized after 48 h aging time and the respective data for reference HAp are shown in Table 2. The refined lattice parameters and *d* spacing values of the HAp samples are in a good agreement with the reference HAp reported from ICDD-JCSd 09-432.

3.2. FTIR spectra

The assignments of the observed vibrational frequencies of dried nano-HAp synthesized using different aging times are summarized in Table 3. Fig. 3 shows the FTIR spectrum of as-dried sample after 48 h aging time. The first indication of the formation of HAp is in the form of broad FTIR band centered around 1000–1100 cm⁻¹ [29]. Furthermore, the peaks around 3570 cm⁻¹ and 630 cm⁻¹ are the characteristic peaks of stoichiometric HAp [30]. The peak at 962 cm⁻¹ [31–34] corresponds to a non-degenerate symmetric stretching mode, ν₁, of the P–O bond in phosphate group. The weak peak at 474 cm⁻¹ [18,20] is the doubly degenerate bending mode, ν₂, of the phosphate group. As a major peak of phosphate group, triply degenerate asymmetric P–O stretching peak, ν₃, which is the most intensified peak among the phosphate vibration modes, could be identified approximately around 1094 cm⁻¹

Table 2

d spacing of the HAp synthesized after 48 h aging time in comparison with the reference JCSd 09-432 HAp card.

hkl	<i>d</i> (nm)		2θ (°)	
	Experimental	Standard HAp	Experimental	Standard HAp
002	0.3445	0.3440	25.843	25.879
102	0.3175	0.3170	28.081	28.126
210	0.3085	0.3080	28.922	28.966
211	0.2816	0.2814	31.748	31.773
112	0.2773	0.2778	32.258	32.196
300	0.2725	0.2720	32.845	32.902
202	0.2633	0.2631	34.024	34.048
310	0.2262	0.2262	39.812	39.818
222	0.1943	0.1943	46.704	46.711
312	0.1892	0.1890	48.051	48.103
213	0.1840	0.1841	49.494	49.468
321	0.1805	0.1806	50.514	50.493
402	0.1755	0.1754	52.055	52.100
004	0.1720	0.1722	53.212	53.143

[31–33,35]. The band between 564 cm⁻¹ and 604 cm⁻¹ [31,33] belongs to triply degenerate ν₄, O–P–O bending mode in the phosphate group, which occupies two sites in the crystal lattice. Two distinguishable splitting of ν₄ vibrations indicate the low site symmetry of molecules, as two peaks confirm the presence of more than one distinct site for the phosphate group in hydroxyapatite lattice [36]. The peaks at 633 and 3564 cm⁻¹ [31–33] are assigned to the librational mode and intramolecular stretching vibration of the hydroxyl group in crystal structure of HAp, respectively. The peak at 1635 cm⁻¹ [37] is signature of the bending mode of hydroxyl group in the adsorbed water. The peak at 3564 cm⁻¹ is assigned to free O–H stretching mode, which may be present on the surface of the crystallites. As the crystallization was carried out in alkaline range (pH = 10.5), dissolving of atmospheric CO₂ yielding CO₃²⁻ based on the peaks at 1422 and 875 cm⁻¹ [38]. The band at 875 cm⁻¹ [36] indicates ν₂ bending mode of CO₃²⁻ group and suggests a B type carbonate substitution. The ν₃ stretching mode of CO₃²⁻ groups was also observed at 1422 cm⁻¹ [39] in the FTIR spectra. The shape of the ν₃ peak and the absence of the C–O absorption band at 700 cm⁻¹ indicate that no calcite was associated with the HAp. Carbonate ions can substitute for either OH⁻ or PO₄³⁻ ions in the apatite structure. Since carbonates are constituents of bone structures [40], the presence of CO₃²⁻ may improve the bioactivity of HAp rather than being a cause of concern.

3.3. Thermogravimetric analysis (TGA/DTA)

The TGA of the dried sample which was aged for 48 h in air was carried out between 30 °C and 1200 °C in nitrogen atmosphere at a

Table 3

Assignments of the observed vibrational frequencies of dried nano-HAp synthesized using different aging times.

Assignments	Observed vibrational frequencies (cm ⁻¹)		
	12 h	24 h	48 h
ν ₁ stretching mode, PO ₄ ³⁻ (w)	962	962	962
ν ₂ bending mode, PO ₄ ³⁻ (w)	474	474	474
ν ₃ stretching mode, PO ₄ ³⁻ (s)	1036–1093	1035–1095	1034–1094
ν ₄ stretching mode, PO ₄ ³⁻ (s,shp)	564–603	565–604	565–603
Librational mode, OH ⁻ (m)	633	633	633
Stretching mode, OH ⁻ (w)	3564	3564	3564
ν ₂ bending mode, H ₂ O (w)	1636	1634	1635
ν ₂ bending mode, CO ₃ ²⁻	875	875	875
ν ₃ stretching mode, CO ₃ ²⁻	1421	1421	1423

w: weak, m: medium, s: strong, shp: sharp.

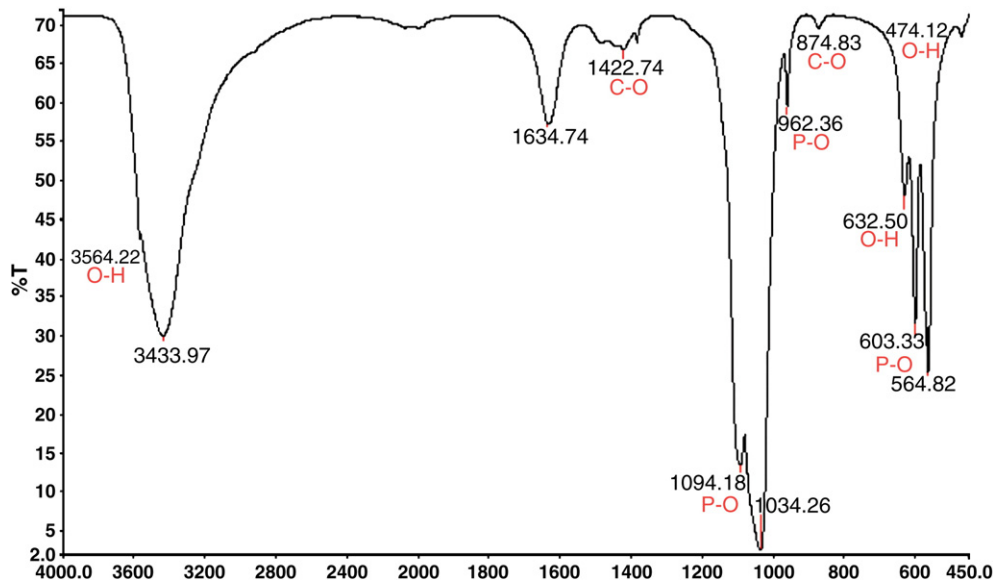


Fig. 3. The FTIR spectrum of as-dried Hap sample after 48 h aging in air.

heating rate of $20\text{ }^{\circ}\text{C min}^{-1}$, as shown in Fig. 4. A steep slope or a sharp weight loss that could be attributed to the decomposition of HAp was not observed in the thermogram and the total weight loss of the sample is found to be 10.52%. This weight loss can be associated to the evaporation of adsorbed and structurally incorporated water and solvent molecules. There is no significant weight loss observed above $600\text{ }^{\circ}\text{C}$, indicating that the synthesized HAp generates a stable phase after heat-treatment at temperatures above $600\text{ }^{\circ}\text{C}$.

3.4. Observation of particle morphology (FEG-SEM)

Surface morphology was observed using two different field-emission SEMs. Prior to the SEM observation, particle surface was vacuum coated with a thin film of platinum. Figs. 5(a) and 6(a) shows the SEM images of the as-dried powder and the powders obtained after heat-treatment at $750\text{ }^{\circ}\text{C}$ for 4 h in stagnant air, respectively. After the heat treatment, the mean particle size and

morphology changes can be clearly observed from SEM micrographs. The sintering process caused not only shrinkage and bending of the needle-like structures, but also the growth of the particle size.

The EDX spectrums of the synthesized powders before and after heat treatment are shown in Figs. 5(b) and 6(b), revealing the elemental composition of nano-HAp. Clear peaks corresponding to Ca, P and O were obtained, as there have been no other significant elements detected. Through this analysis, the Ca/P ratio was calculated to be approximately 1.70, confirming the purity of HAp.

3.5. TEM analysis

In addition to the TEM bright field images, selected area electron diffraction patterns (SAED) were also measured for dried and sintered HAp. Using the diffraction pattern of the nano-crystal we can determine its orientation with respect to the electron beam and to any adjacent crystals. The positions of the allowed hkl reflections are characteristic

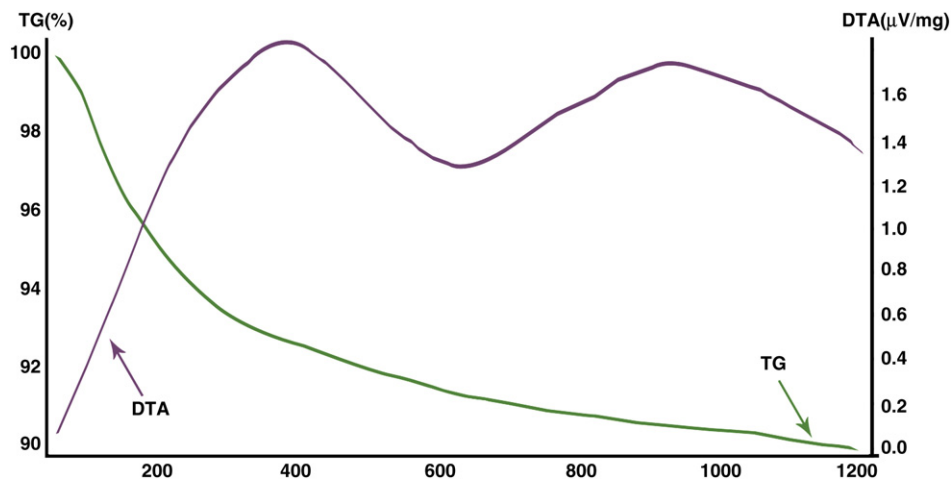


Fig. 4. TGA/DTA of the as-dried Hap sample.

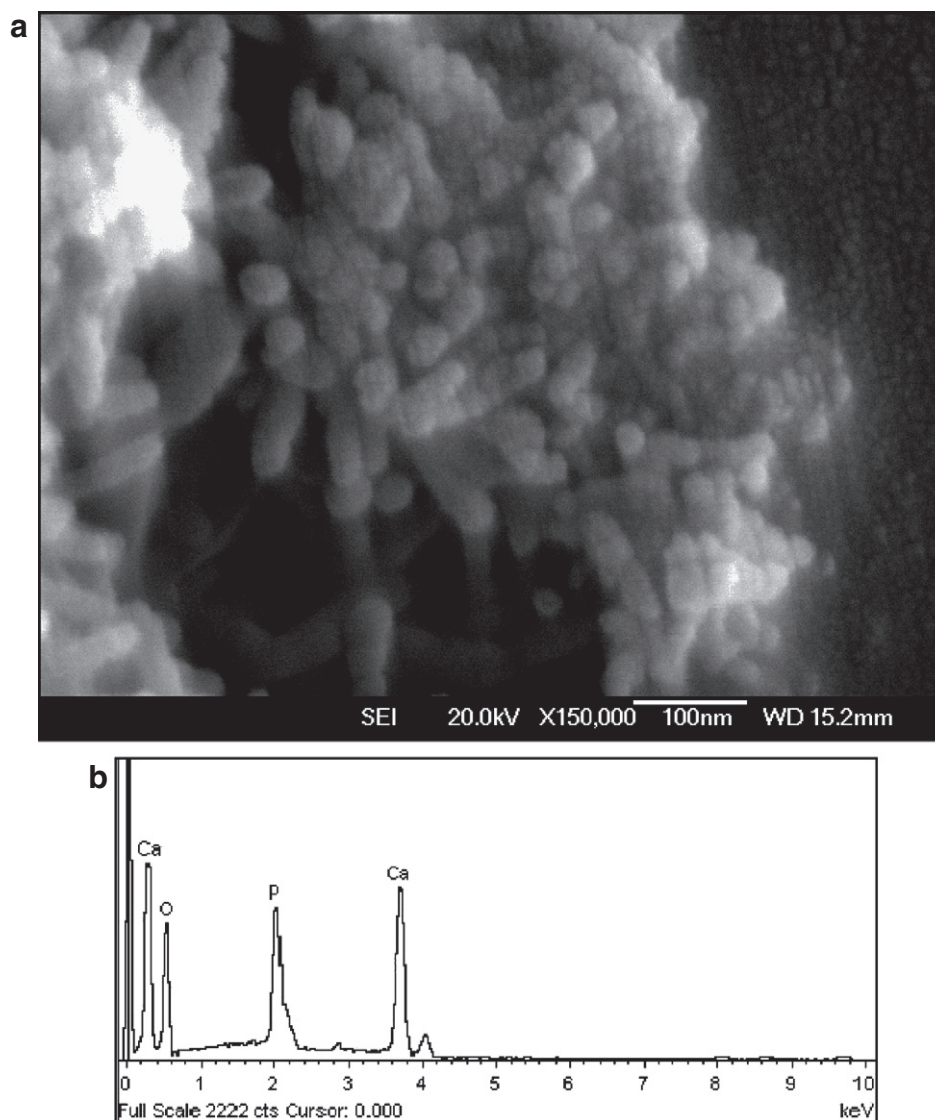


Fig. 5. SEM micrograph (a) and energy dispersive X-ray analysis spectrum (b) of as-dried HAp synthesized aged for 24 h in air.

to the crystal system. From the indexing of the spots, the orientation of the crystal in terms of the zone axis [UVW] in which the indexed planes lie can be deduced [41].

In the TEM micrographs, needle-like nano-HA crystals with the average particle diameters ranging from 9–15 nm were observed and this may suggest that the sintering process promotes the particle growth and agglomeration. The distance between crystal planes was measured using the standard, indexed, diffraction patterns for hcp crystals in the beam directions taking the ratios of the principal spot spacing into consideration, as well as the angles between the principal plane normal.

Fig. 7(a) and (b) shows the TEM micrograph and SAED of the dried HAp synthesized after using 24 h aging time. The HAp sample showed nano-sized needle-like morphology with a mean particle size of 12 nm in diameter. The inter-planar spacing taken from the [0110] zone axis along the [2110] direction was measured to be ~ 3.3 Å (a) and from the [1213] zone axis and along the [1101] direction was measured to be ~ 3.9 Å (b). The ring pattern and the fast Fourier transform image can also be seen in Fig. 7(b). The TEM micrograph and SAED of the same HAp sample sintered at 750 °C is

presented in Fig. 8. Due to the agglomeration and crystal growth, the mean particle size is 50 nm. The inter-planar spacing taken from the [1213] zone axis along the [1010] direction was measured to be ~ 3.1 Å.

4. Conclusions

We have successfully developed a novel method to synthesize pure, hexagonal, needle-like and thermally stable nano-HAP powder at a lower temperature than the other existing methods in literature [3,14–26]. More importantly, in this novel and simple alcohol based process, gel formation was obtained without using any catalyst and nano-HAP was synthesized without any need of grinding process. XRD, FTIR, TG-DTA, SEM, and TEM have been used for atomic scale characterization. The nano-crystalline structure has been determined by XRD, FEG-SEM and HR-TEM micrographs. From the SEM and TEM micrographs, the apatitic structure was identified to be hexagonal nano-needle like with a 12 nm mean particle diameter and 65 nm mean particle length. XRD results revealed that the $\text{Ca}_3(\text{PO}_4)_2$ evolves as an impurity phase if aging time is not sufficient and the pure HAP

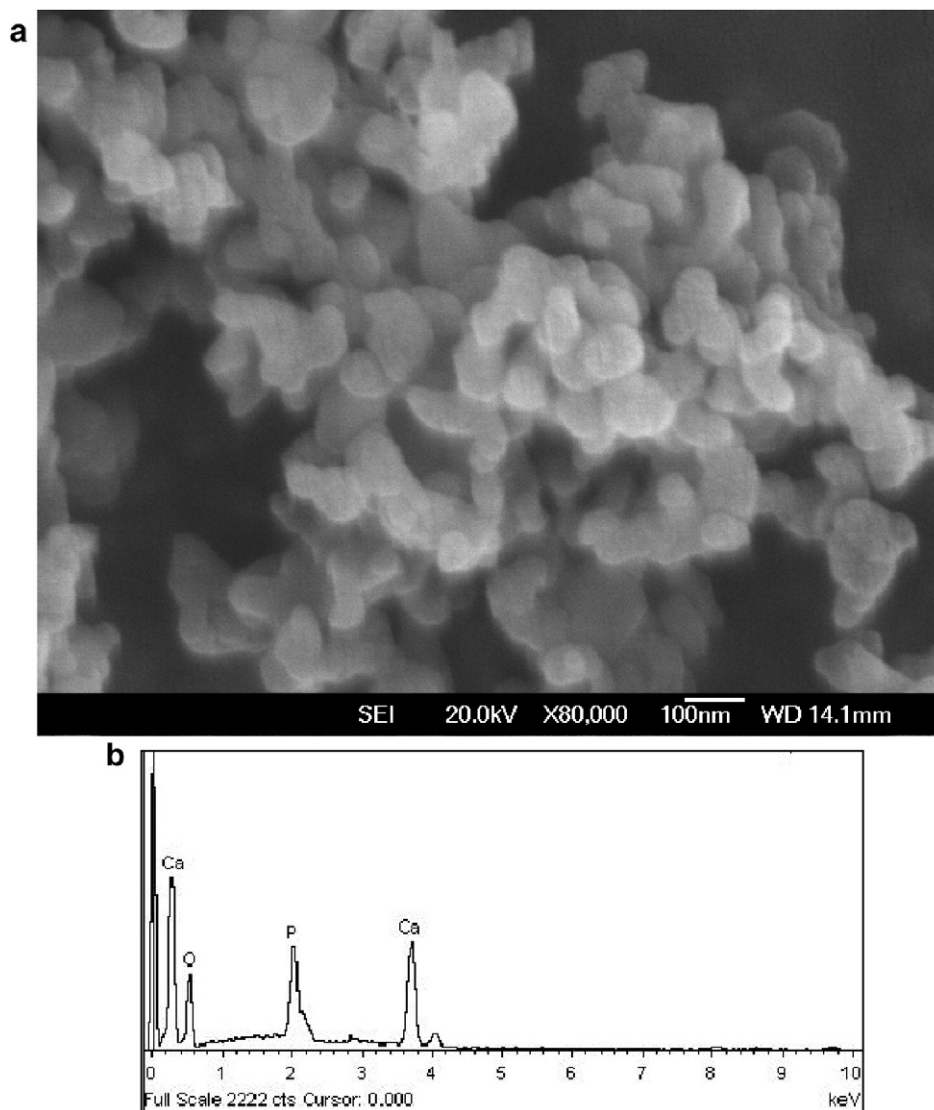


Fig. 6. SEM micrograph (a) and energy dispersive X-ray analysis (b) spectrum of HAp sintered at 750 °C and aged for 24 h in air.

could be obtained after 48 h aging time. In addition to the characteristic peaks of the stoichiometric HAp, peaks, which belong to the carbonate groups, were also observed in the FTIR spectra. As carbonates are constituents of bone structures, the presence of these might even be more advantageous to improve the bioactivity of HAp.

The proposed method is very simple and inexpensive. Therefore, it can be suggested for preparing pure, stoichiometric, nano crystalline HAp, needed for the large-scale productions of various biomaterial applications.

Acknowledgments

The authors would like to thank Dr. Hatice Bayrakçeken for the TGA analysis. Feray Bakan is grateful to the Scientific and Technological Research Council of Turkey (TÜBİTAK) for financial support through National Scholarship Programme for PhD students.

References

- [1] M. Jarcho, Calcium phosphates ceramics as hard tissues prosthetics, *Clinical Orthopaedics and Related Research* 157 (1981) 259.
- [2] K. De Groot, P. Ducheyne, *In vivo* surface activity of a hydroxyapatite alveolar bone substitute, *Journal of Biomedical Materials Research* 15 (1981) 441.
- [3] G. Bezzi, G. Celotti, E. Landi, T.M.G. La Torretta, I. Sopyan, A. Tampieri, A novel sol-gel technique for hydroxyapatite preparation, *Materials Chemistry and Physics* 78 (2003) 816.
- [4] S.J. Kalita, H.A. Bhatt, Nanocrystalline hydroxyapatite doped with magnesium and zinc: synthesis and characterization, *Materials Science and Engineering C* 27 (2007) 837.
- [5] K. Cheng, W. Weng, G. Han, P. Du, G. Shen, J. Yang, J.M.F. Ferreira, Sol-gel derived fluoridated hydroxyapatite films, *Materials Research Bulletin* 38 (2003) 89.
- [6] Peipei Wang, Caihong Li, Haiyan Gong, Xuerong Jiang, Hongqiang Wang, Kaixing Li, Effects of synthesis conditions on the morphology of hydroxyapatite nanoparticles produced by wet chemical process, *Powder Technology* 20 (3) (2010) 315.
- [7] E.K. Girija, G. SureshKumar, A. Thamizhavel, Y. Yokogawa, S. NarayanaKalkura, Role of material processing on the thermal stability and sinterability of nanocrystalline hydroxyapatite, *Powder Technology* 225 (2012) 190.
- [8] A.K. Nayak, Hydroxyapatite synthesis methodologies: an overview, *International Journal of ChemTech Research* 2 (2) (2010) 903.
- [9] E.A. Abdel-Aal, A.A. El-Midany, H. El-Shall, Mechanochemical-hydrothermal preparation of nano-crystallite hydroxyapatite using statistical design, *Materials Chemistry and Physics* 112 (2008) 202.
- [10] M. Nabil Salimi, Rachel H. Bridson, Liam M. Grover, Gary A. Leeke, Effect of processing conditions on the formation of hydroxyapatite nanoparticles, *Powder Technology* 218 (2012) 109.
- [11] H. Eshtiagh-Hosseini, M.R. Housaindokht, M. Chahkandi, Effects of parameters of sol-gel process on the phase evolution of sol-gel-derived hydroxyapatite, *Materials Chemistry and Physics* 106 (2007) 310.
- [12] P. Li, K. de Groot, Better bioactive ceramics through sol-gel process, *Journal of Sol-Gel Science and Technology* 2 (1994) 797.
- [13] D. Liu, T. Troczynski, W.J. Tseng, Water-based sol-gel synthesis of hydroxyapatite: process development, *Biomaterials* 22 (2001) 1721.

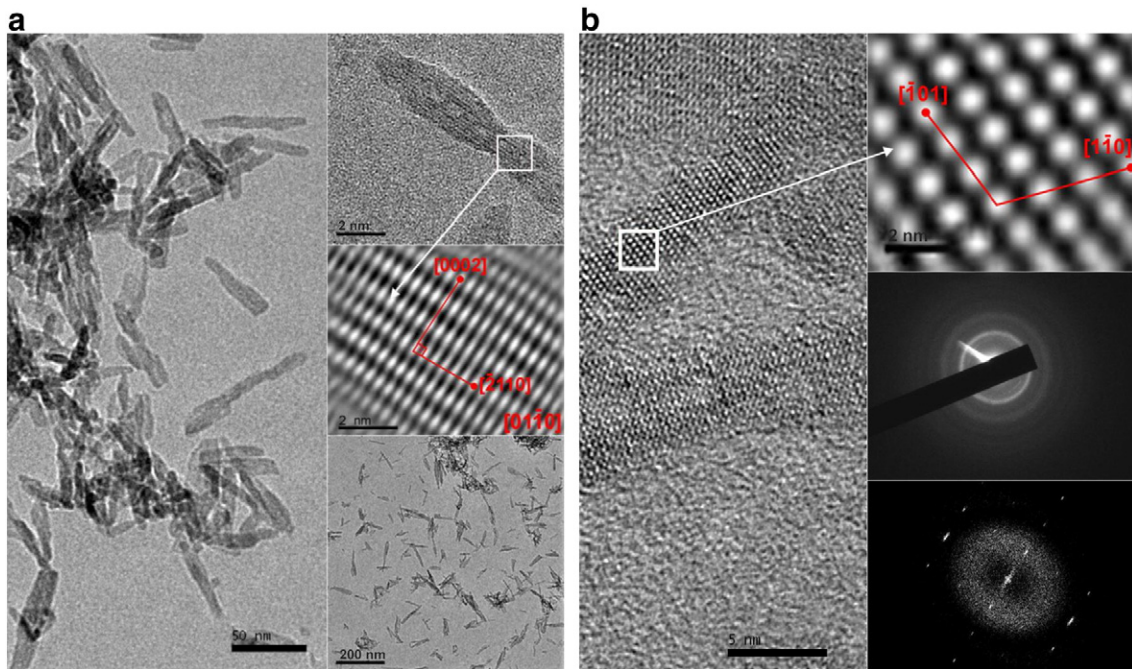


Fig. 7. (a) TEM micrograph and SAED of the dried HAp, aged for 24 h in air. (b) TEM micrograph and SAED of the dried HAp, aged for 24 h in air.

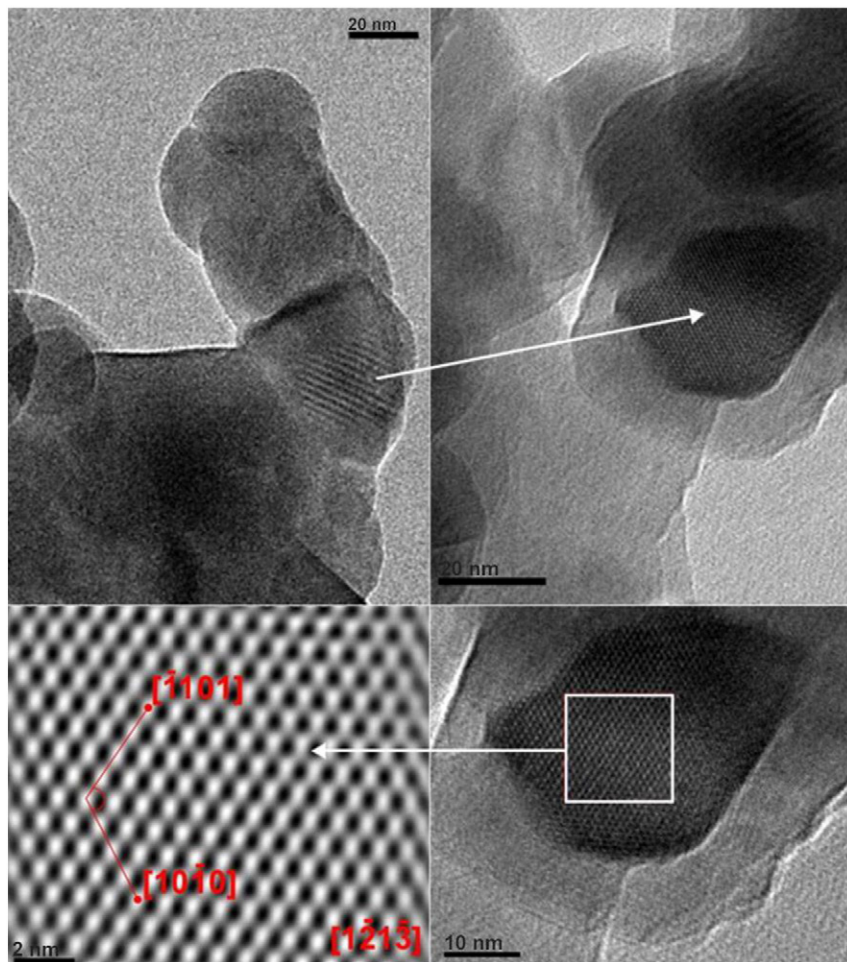


Fig. 8. The TEM micrograph and SAED of the HAp sample sintered at 750 °C.

- [14] T.A. Kuriakose, S.N. Kalkuraa, M. Palanichamy, D. Arivuoli, K. Dierkse, G. Bocellif, C. Betzelb, Synthesis of stoichiometric nano crystalline hydroxyapatite by ethanol-based sol–gel technique at low temperature, *Journal of Crystal Growth* 263 (2004) 517.
- [15] L. Yang, X.S. Ning, W.W. Jia, K.X. Chen, H.P. Zhou, Particle size control in sol gel synthesis of nano hydroxyapatite, *Journal Advanced Materials Research* 11–12 (2006) 231.
- [16] M. Bilton, A.P. Brown, S.J. Milne, Sol–gel synthesis and characterisation of nano-scale hydroxyapatite, *Journal of Physics Conference Series* 241 (1) (2010) 012052.
- [17] A. Ruban Kumar, S. Kalainathan, Sol–gel synthesis of nanostructured hydroxyapatite powder in presence of polyethylene glycol, *Physica B: Physics of Condensed Matter* 405 (2010) 2799.
- [18] Y. Liu, W. Wang, Y. Zhan, C. Zheng, G. Wang, A simple route to hydroxyapatite nanofibers, *Materials Letters* 56 (2002) 496.
- [19] A. Milev, G.S.K. Kannangara, B. Ben-Nissan, Morphological stability of hydroxyapatite precursor, *Materials Letters* 57 (2003) 1960.
- [20] Y. Han, S. Li, X. Wang, X. Chen, Synthesis and sintering of nanocrystalline hydroxyapatite powders by citric acid sol–gel combustion method, *Materials Research Bulletin* 39 (2004) 25.
- [21] I. Bogdanoviciene, A. Beganskiene, K. Tönsuaadu, J. Glaser, H.-Jürgen Meyer, A. Kareiva, Calcium hydroxyapatite, Ca₁₀(PO₄)₆(OH)₂ ceramics prepared by aqueous sol–gel processing, *Materials Research Bulletin* 41 (2006) 1754.
- [22] Dean-Mo Liu, T. Troczynski, W.J. Tseng, Water-based sol–gel synthesis of hydroxyapatite: process development, *Biomaterials* 2 (2) (2001) 1721.
- [23] S. Jadalannagari, S. More, M. Kowshik, S.R. Ramanan, Low temperature synthesis of hydroxyapatite nano-rods by a modified sol -gel technique, *Materials Science and Engineering C* 31 (2011) 1534–1538.
- [24] W. Feng, L. Mu-sen, L. Yu-peng, Q. Yong-xin, A simple sol–gel technique for preparing hydroxyapatite nanopowders, *Materials Letters* 59 (2005) 916.
- [25] U. Vijayalakshmi, K. Prabhakaran, S. Rajeswari, Preparation and characterization of sol-gel hydroxyapatite and its electrochemical evaluation for biomedical applications, *Journal of Biomedical Materials Research. Part A* 87 (2008) 739.
- [26] M. Bilton, A.P. Brown, S.J. Milne, Sol–gel synthesis and characterization of nano-scale hydroxyapatite, *Journal of Physics Conference Series* 241 (2010) 012052.
- [27] L.A. Azaroff, *Elements of X-ray Crystallography*, McGraw-Hill, New York, 1968.
- [28] X. Wei, C. Fu, K. Savino, M.Z. Yates, Fully dense yttrium-substituted hydroxyapatite coatings with aligned crystal domains, *Crystal Growth and Design* 12 (1) (2012) 217.
- [29] H.K. Varma, S.S. Babu, Synthesis of calcium phosphate bioceramics by citrate gel pyrolysis method, *Ceramics International* 31 (2005) 109.
- [30] W.L. Suchanek, P. Shuk, K. Byrappa, R.E. Riman, K.S. Ten Huisen, V.F. Janes, Mechanochemical–hydrothermal synthesis of carbonated apatite powders at room temperature, *Biomaterials* 23 (2002) 699.
- [31] B.O. Fowler, Infrared studies of apatites. I. Vibrational assignments for calcium, strontium, and barium hydroxyapatites utilizing isotopic substitution, *Inorganic Chemistry* 13 (1974) 194.
- [32] S.J. Gadaleta, E.P. Paschalis, N.P. Camacho, F. Betts, R. Mendelshon, A.L. Boskey, Fourier transform infrared spectroscopy of synthetic and biological apatites, in: Z. Amjad (Ed.), *Mineral scale formation and inhibition*, Plenum Press, New York, 1995.
- [33] W.E. Klee, G. Engel, Infrared spectra of the phosphate ions in various apatites, *Journal of Inorganic and Nuclear Chemistry* 32 (1970) 1837.
- [34] C.B. Baddiel, E.E. Berry, Spectra–structure correlations in hydroxyapatite and fluorapatite, *Spectrochimica Acta. Part A, Molecular and Biomolecular Spectroscopy* 22 (1966) 1407.
- [35] S.J. Joris, C.H. Amberg, Nature of deficiency in nonstoichiometric hydroxyapatites. II. Spectroscopic studies of calcium and strontium hydroxyapatites, *Journal of Physical Chemistry* 75 (1971) 3172.
- [36] I. Rehman, W. Bonfield, Characterization of hydroxyapatite and carbonated apatite by photo acoustic FTIR spectroscopy, *Journal of Materials Science. Materials in Medicine* 8 (1997) 1–4.
- [37] T. Anee Kuriakose, S. Narayana Kalkura, M. Palanichamy, D. Arivuoli, Karsten Dierks, G. Bocelli, C. Betzel, Synthesis of stoichiometric nano crystalline hydroxyapatite by ethanol-based sol–gel technique at low temperature, *Journal of Crystal Growth* 263 (2004) 517.
- [38] J.C. Elliot, *Structure and Chemistry of the Apatites and Other Calcium Ortho Phosphates*, Elsevier, Amsterdam, 1994.
- [39] A. Ślósarczy, Z. Paszkiewicz, C. Paluszkiwicz, FTIR and XRD evaluation of carbonated hydroxyapatite powders synthesized by wet methods, *Journal of Molecular Structure* 744 (2005) 657.
- [40] R. Murugan, S. Ramakrishna, Development of nano composites for bone grafting, *Composites Science and Technology* 65 (2005) 2385.
- [41] D.B. Williams, C.B. Carter, *Transmission electron microscopy, A Textbook for Materials Science*, Springer, New York, 2009.